NRC Publications Archive
Archives des publications du CNRC

Variable stars in Local Group Galaxies: I. Tracing the early chemical enrichment and radial gradients in the Sculptor dSph with RR Lyrae stars

Martínez-vázquez, C. E.; Monelli, M.; Bono, G.; Stetson, P. B.; Ferraro, I.; Bernard, E. J.; Gallart, C.; Fiorentino, G.; Iannicola, G.; Udalski, A.

National Research Council Canada
Conseil national de recherches Canada

Canada

Variable stars in Local Group Galaxies – I. Tracing the early chemical enrichment and radial gradients in the Sculptor dSph with RR Lyrae stars

C. E. Martínez-Vázquez,[1,2]* M. Monelli,[1,2]* G. Bono,[3,4]* P. B. Stetson,[5] I. Ferraro,[4] E. J. Bernard,[6] C. Gallart,[1,2] G. Fiorentino,[7] G. Iannicola[4] and A. Udalski[8]

[1]*IAC – Instituto de Astrofísica de Canarias, Calle Vía Lactea s/n, E-38205 La Laguna, Tenerife, Spain*
[2]*Departmento de Astrofísica, Universidad de La Laguna, E-38200 La Laguna, Tenerife, Spain*
[3]*Department of Physics, Università di Roma Tor Vergata, via della Ricerca Scientifica 1, I-00133 Roma, Italy*
[4]*INAF–Osservatorio Astronomico di Roma, via Frascati 33, I-00040 Monte Porzio Catone, Italy*
[5]*NRC–Herzberg, Dominion Astrophysical Observatory, 5071 West Saanich Road, Victoria, BC V9E 2E7, Canada*
[6]*Institute for Astronomy, University of Edinburgh, Royal Observatory, Blackford Hill, Edinburgh EH9 3HJ, UK*
[7]*INAF–Osservatorio Astronomico di Bologna, via Ranzani 1, I-40127 Bologna, Italy*
[8]*Warsaw University Observatory, Al. Ujazdowskie 4, PL-00-478 Warszawa, Poland*

ABSTRACT

We identified and characterized the largest (536) RR Lyrae (RRL) sample in a Milky Way dSph satellite (Sculptor) based on optical photometry data collected over ∼24 years. The RRLs display a spread in *V*-magnitude (∼0.35 mag) which appears larger than photometric errors and the horizontal branch (HB) luminosity evolution of a mono-metallic population. Using several calibrations of two different reddening free and metal independent period–Wesenheit relations we provide a new distance estimate $\mu = 19.62$ mag ($\sigma_\mu = 0.04$ mag) that agrees well with literature estimates. We constrained the metallicity distribution of the old population, using the M_I period–luminosity relation, and we found that it ranges from -2.3 to -1.5 dex. The current estimate is narrower than suggested by low and intermediate spectroscopy of RGBs (Δ [Fe/H]≤ 1.5). We also investigated the HB morphology as a function of the galactocentric distance. The HB in the innermost regions is dominated by red HB stars and by RRLs, consistent with a more metal-rich population, while in the outermost regions it is dominated by blue HB stars and RRLs typical of a metal-poor population. Our results suggest that fast chemical evolution occurred in Sculptor, and that the radial gradients were in place at an early epoch.

Key words: stars: variables: RR Lyrae – galaxies: evolution – galaxies: individual: Sculptor dSph – Local Group – galaxies: stellar content.

1 INTRODUCTION

Understanding the evolution of Local Group dwarf galaxies offers a fundamental key to constrain the early formation and evolution of cosmic structures (e.g. Mayer 2010; Madau & Dickinson 2014). Current ground-based and space facilities allow us to resolve their stellar content and to provide a wealth of observables to reconstruct their star formation history and chemical enrichment (Gallart, Zoccali & Aparicio 2005; Tolstoy, Hill & Tosi 2009).

RR Lyrae (RRL) stars are reliable distance indicators, since their individual distances can be estimated using either the different developments of the Baade–Wesselink method (Storm et al. 2004), the correlation between visual magnitude and Fe abundance (Cacciari & Clementini 2003), statistical parallaxes (Dambis, Rastorguev &

Zabolotskikh 2014), optical, near-infrared (NIR) and mid-infrared (MIR) period–luminosity–metallicity (PLZ; Bono et al. 2001, 2003; Catelan, Pritzl & Smith 2004) and the reddening free period–Wesenheit–metallicity (PWZ; Braga et al. 2015; Coppola et al. 2015). The above diagnostics all have pros and cons, but during the last few years the use of accurate and precise NIR and MIR mean magnitudes has provided a new spin on the use of RRLs as distance indicators (Madore et al. 2013; Klein et al. 2014; Neeley et al. 2015). This evidence was soundly complemented by the recent estimates of the trigonometric parallaxes for five field RRLs using the FGS on board of HST (Benedict et al. 2011). Moreover, the use of the reddening free magnitudes, the so-called period–Wesenheit relation (PWR) is firmly supported by theory (Marconi et al. 2015) and observations (Braga et al. 2015).

RRL stars also play a fundamental role as stellar tracers. Theory and observations indicate that they are present in all stellar systems hosting an old (>10 Gyr) stellar population. They are

*⋆ E-mail: clara.marvaz@gmail.com (CEM-V); monelli@iac.es (MM); bono@roma2.infn.it (GB)

low-mass (0.6–0.8 M$_\odot$) central helium-burning stars in their Horizontal Branch (HB) evolutionary phase. This ancient population is the fossil record of the early stages of galaxy evolution and provides firm constraints on the time-scale of their early formation and evolution.

In this context, Sculptor is an interesting laboratory, since it hosts a conspicuous old stellar population, but its star formation is quite complex (Da Costa 1984; Majewski et al. 1999; Tolstoy et al. 2004; de Boer et al. 2012). Moreover, Sculptor appears to be characterized by a complicated chemical enrichment history (Smith & Dopita 1983; Majewski et al. 1999; Hurley-Keller, Mateo & Grebel 1999; Starkenburg et al. 2013). In particular, the presence of a large metallicity spread has been suggested in this galaxy. Detailed spectroscopic measurements (Tolstoy et al. 2004; Walker et al. 2007, 2009) showed not only that the more metal-rich red giant branch (RGB) stars ([Fe/H] > −1.7) are more centrally concentrated than more metal-poor ones, leading to a significant metallicity gradient, but also that they have different kinematics. More importantly, the fact that red HB (RHB) stars are more centrally concentrated than blue HB (BHB) stars suggests that a spread in metallicity is also present in the old stellar component (HB stars), which in turn suggests a relatively fast early chemical evolution. Since the stars that are now RRL stars were formed during an even shorter time than the global HB population, observing a gradient in their pulsational properties would put even more stringent constraints on the time-scale of the chemical enrichment in Sculptor (Bernard et al. 2008).

Since the discovery of Sculptor by Shapley (1938), a number of estimates of its distance have been proposed in the literature. After the initial approximate value by Shapley (1938) based on photographic data, the first accurate measurement dates back to the work of Hodge (1965) who derived a true distance modulus of 19.7 ± 0.15 mag using three different methods (luminosity of the RGB, two W Virginis, and three RRL stars). Kunkel & Demers (1977) provided distance estimates based on the average magnitude of 24 stars on the HB with colours covering the RR Lyrae gap (0.15 < (B–V)$_0$ < 0.52); they found a true distance modulus of 19.47 ± 0.10 mag, slightly lower than the previous one.

More recently, Pietrzynski et al. (2008) provided a distance value of $\mu = 19.67 \pm 0.14$ mag by applying different theoretical and empirical calibrations of the PLZ relation for RRLs in the NIR (J, K) magnitudes, consistent with the V-band data of RRLs and also in very good agreement with the results obtained by Rizzi (2002) based on the tip of RGB (TRGB, 19.64 ± 0.08 mag) and HB stars (19.66 ± 0.15) based on optical photometry.

The search for variable stars in Sculptor dates back to more than half a century ago (Baade & Hubble 1939; Thackeray 1950). The first systematic search was performed by van Agt (1978), who identified more than 600 candidate variable stars, but provided periods only for ~10 per cent of the sample.

The most complete RRL catalogue to date was provided by Kaluzny et al. (1995) based on the OGLE-I survey observations (Udalski et al. 1992). They investigated the central region of Sculptor (15 arcmin ×15 arcmin) and identified and characterized 226 RRLs. Their pulsation properties are consistent with metal-poor chemical composition ([Fe/H] < −1.7) and a spread in metallicity. The spectroscopic follow-up by Clementini et al. (2005) confirmed this preliminary evidence based on low resolution (LR) spectra of 107 RRLs. In particular, they found that the metallicity distribution peaks at [Fe/H] ~ −1.8, but covers more than 1.5 dex (−2.4 ≤ [Fe/H]≤ −0.8).

We take advantage of a large sample of RRLs, including some new discoveries, to provide a revised distance estimate for Sculptor and to constrain the parameters of an early chemical enrichment. The current sample is a factor of 2 larger than previously analysed ones (536 versus 216[1]). Moreover, we provide pulsation period, mode and mean magnitudes in three different photometric bands (see Section 2). In Section 4 we describe the approach for the new distance determination, while in Section 5 we investigate the spread in metallicity of the old stellar population using the *I*-band period–metallicity relation of RRLs.

2 PHOTOMETRIC DATA SET AND RR LYRAE IDENTIFICATION

We used 4404 calibrated images from the photometric data base collected by one of us (PBS), covering an extended area around the Sculptor dSph. The time baseline of these data is nearly 24 years (from 1987 October until 2011 August). These data are individual CCD images from many ground-based telescopes: CTIO 0.9 m+[TI, Tek2K], LCO 1.0 m+FORD2 (OGLE-I survey), MPI/ESO 2.2m+WFI, ESO NTT 3.6m+SUSI, CTIO 4m+Mosaic2, SOAR 4.1 m+SOI. The full data set covers an area of ~6 deg.^{2} centred on the Sculptor dSph galaxy. However, only the central region (~3 deg.^{2}) could be properly calibrated. The DAOPHOT/ALLFRAME package of programs (Stetson 1987, 1994) was used to obtain the instrumental photometry of the stars. A detailed description of the observations and data reduction will be given in a forthcoming paper.

We performed the variability search over the full data set. An updated version of the Welch-Stetson variability index (Welch & Stetson 1993) was used to identify candidate variable stars on the basis of our multiband photometry. From the list of 663 variable star candidates, we have found 611 actual variable stars and 23 possible variable stars. Out of these real variables, 536 pulsating stars are located in the Instability Strip (IS) of a very extended HB of the Sculptor dSph galaxy, with periods between 0.2 and 1.2 d. Out of these, 82 RRLs are new identifications, and for 320 RRLs all their pulsational parameters (period, mean magnitude, and amplitude) are derived for the first time. This work increases by over a factor of 2 the number of the known RRL to date in the Sculptor dSph. Our sample includes 216 RRLs of Kaluzny et al. (1995).

We derived pulsational properties for all the RRL stars from our *BVI*-Johnson/Cousins photometry. The search for the period was carried out using a simple string-length algorithm (Stetson et al. 1998). Then a robust least-squares fit of a Fourier series to the data refined the periods. The intensity-averaged magnitudes and amplitudes of the mono-periodic light curves were obtained by fitting the light curves with a set of templates partly based on the set of Layden et al. (1999) following the same method described in Bernard et al. (2009). Thus, through the period and light-curve shape, we identified: (i) 289 *RRab*, pulsating in the fundamental mode; 20 of which are suspected Blazhko, (Blazhko 1907); (ii) 197 *RRc*, pulsating in the first-overtone mode; and (iii) 50 possible multimode *RRd* stars, pulsating in both modes simultaneously, although the classification in some cases was uncertain due to their relatively noisy or (very) poor light curves. The mean (maximum) number of points in the light curves of the RRL stars are 83, 52, and 21 (115, 182 and 28) respectively in *B*, *V*, and *I*.

---

[1] 10 out of the 226 RRLs published by Kaluzny et al. (1995) turned out to be either double identifications or non-variables stars.

3 RR LYRAE INSTABILITY STRIP

The top-left panel Fig. 1 shows the (*B–V, V*) colour–magnitude diagram (CMD) of Sculptor zoomed on the HB region. Data plotted in this CMD show a complex morphology with well defined BHB and RHB stars (black dots) and a large sample of RRLs. The latter group shows several interesting features.(i) The RRL IS is well populated over the entire colour range typical of *RRc* and *RRab* variables.(ii) The spread in magnitude of RRLs is ∼0.35 mag, significantly larger than the typical uncertainty in the mean magnitudes ($\sigma = 0.03$ mag) and significantly larger than the expected from the evolution of a mono-metallic population. The top-right panel of Fig. 1 shows the visual magnitude distribution of the RRLs located within 2.5σ of the average. We ended up with a sample of 520 RRLs and neglected 16 outliers. Using the period-amplitude distribution and by visual inspection of the individual light curves we identified 276 *RRab* + 195 *RRc* (defined by us as *full* sample) and 49 candidate *RRd* variables. (iii) The magnitude distribution of the RRLs is broad and possibly double peaked (see top-left panel).

A plausible working hypothesis to account for the observed spread in magnitude of RRLs is that Sculptor RRLs cover a broad range in metallicity. Using classical luminosity-metallicity relations $M_V(RRL) = \alpha + \beta \cdot$ [Fe/H] by Clementini et al. (2003) and Bono

Figure 2. Optical (B-V, V) CMDs of Sculptor, zoom-in on HB stars. The grey circles display the RRL variable stars of the *full sample* (same as top-left panel in Fig. 1). The red lines show the zero age horizontal branch (ZAHB) from the BaSTI library (Pietrinferni et al. 2004) for different metallicities: $Z = 0.0001$ (left), $Z = 0.0003$ (middle), and $Z = 0.0006$ (right). The black lines display the corresponding evolutionary HB models with the labelled masses, where the overplotted circles indicate time intervals of 10 Myr. The stellar mass, at the typical colours of the RR Lyrae stars, steadily increases when moving from the brightest to the faintest HB models.

et al. (2003), we found that a spread in *V*-magnitude of 0.35 mag implies a range in Fe abundance of the order of ∼0.6 dex. Note that this range has to be treated with caution, since the above relations are prone to systematic uncertainties, and in particular to evolutionary effects (Bono et al. 2001, 2003).

In order to search for possible metallicity trends, we split the sample of RRab and RRc stars into two groups – candidate RRd might have less accurate mean magnitudes and were thus neglected. We have used the mean magnitude of the entire sample, $<V> = 20.13$ ($\sigma = 0.09$) mag, as the limit, shown by a solid line on the left-hand panel and the arrow on the right-hand panel of Fig. 1. We note that this selection is marginally affected by the curvature of the HB, in particular for the bluer stars, but that the results did not change significantly with a different criterion. We find 184 bright (Bt; blue symbols) and 287 faint (Ft; orange symbols) RRLs.

A more restrictive selection based on the quality of the phase coverage of the photometry over the entire pulsation cycle yielded similar results. This refined sample contains 290 RRLs that we defined as the *clean* sample. Among them we have 167 *RRab* and 123 *RRc* variables. Data plotted in the bottom panels of Fig. 1 indicate that the global properties are quite similar to the *full* sample, and indeed the mean *V* magnitude is $<V> = 20.14(\sigma = 0.07)$ mag. The same conclusion applies to the mean *V* magnitude of both Bt- and Ft-RRLs (see labelled values).

In order to rule out the hypothesis that evolutionary effects can explain the observed luminosity range, Fig. 2 shows a comparison with stellar evolutionary tracks for different metallicities. The current predictions come from the BaSTI library (Pietrinferni et al. 2004), they have been computed assuming a scaled-solar chemical mixture (using the α enhanced HB models provide consistent results). They were plotted assuming the reddening law from Cardelli, Clayton & Mathis (1989) and assuming a true distance modulus of $\mu = 19.62$ mag (see Section 4) and a reddening of 0.018 mag. The three panels present the case for $Z = 0.0001, 0.0003, 0.0006$. In
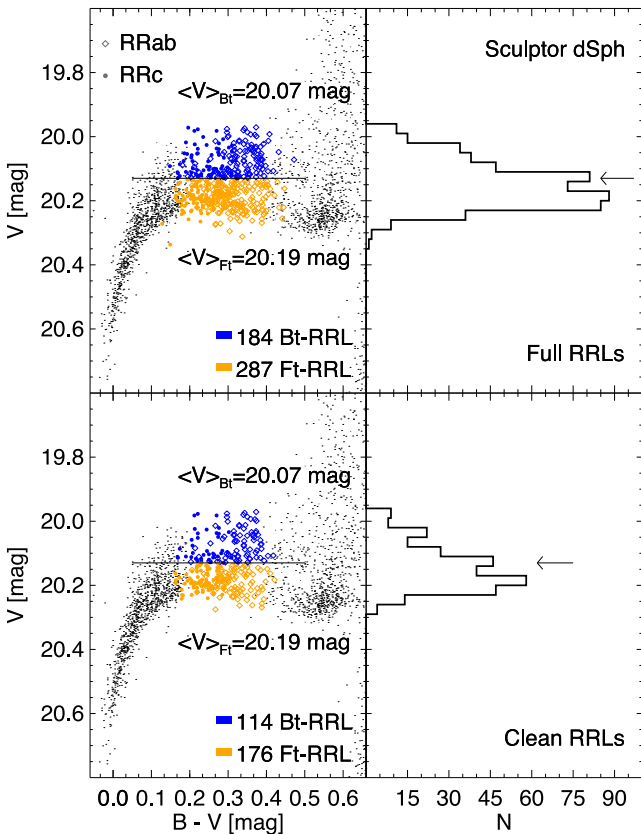

Figure 1. Top-left. Optical (*B–V, V*) CMD of Sculptor, zoom-in on HB stars. Blue and orange symbols display bright and faint RRLs of the *full* sample. The horizontal line shows the mean magnitude of the *full* sample (*V*= 20.13 mag) adopted to split the bright and faint samples. Diamonds and circles display *RRab* and *RRc* variables. The number of RRLs in each subsample is labelled. Bottom-left. Same as the top, but for the clean sample. Top-right. *V*-band luminosity distribution of RRLs. The arrow marks the magnitude adopted to split bright and faint RRLs. Bottom-right. Same as the top, but for the clean sample. For the sake of clarity, *RRd* are not represented.
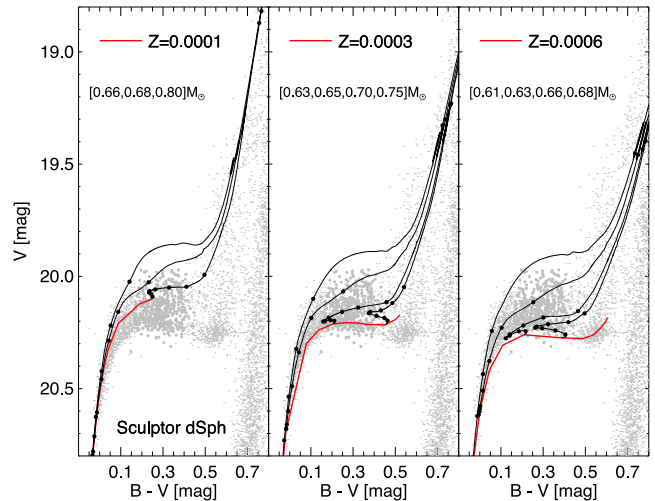
each panel the red thick line shows the Zero Age Horizontal Branch (ZAHB), while individual evolutionary tracks for selected labelled masses are presented by the thin black lines. The black circles mark the points of each tracks with a time step of 10 Myr after the helium ignition. Overall, the figure shows many interesting points:

(i) The luminosity of HB stars mainly depends on the metallicity, therefore it is plausible to assume that the faint sample previously selected includes the most metal-rich RRL stars, while the bright sample should include the more metal-poor stars. However, off-ZAHB evolution could move more metal-rich stars into the bright sample.

(ii) The comparison with tracks with $Z = 0.0006$, in the right-hand panel, suggests that this is a fair upper limit to the RRL metallicity. Nevertheless, the ZAHB is not able to well reproduce the RHB, suggesting that even more metal-rich stars populate this feature of the CMD.

(iii) The left-hand panel ($Z = 0.0001$) shows that very metal-poor stars are expected to start core helium-burning on the blue side of the IS, except possibly the most massive ones. Nevertheless, the stars evolving off the ZAHB do cross the IS, although this occurs at relatively bright luminosity where only a few very bright RRL stars are observed. Moreover, the spacing between black points indicates that the crossing of the IS is an extremely rapid phase, thus very difficult to observe. This is expected to be even more effective for extremely metal poor stars ($Z < 0.0001$). Therefore, although possible, it seems unlikely that many of the Sculptor RRL stars are as metal-poor as the most metal-poor stars detected in the RGB (Starkenburg et al. 2013).

(iv) While the tracks corresponding to each metallicity cover a significant range of luminosity, it is clear that the luminosity spread associated with the evolutionary effects of a mono-metallic population is not sufficient to explain the observed magnitude range of RRL stars. This strongly supports our hypothesis that the RRLs in Sculptor cover a wide range of metallicities.

4 DISTANCE DETERMINATION

The evidence that the RRLs in Sculptor show a spread in chemical composition is a thorny problem for distance determinations. The diagnostics adopted to estimate individual RRL distances depend on the Fe content (see Section 1). However, recent theoretical (Marconi et al. 2015) and empirical (Braga et al. 2015; Coppola et al. 2015) evidence indicates that the period–Wesenheit relation (PWR) in the (V, B–V) and the (V, B–I) bands are minimally affected by metallicity. The above Wesenheit magnitudes are defined as $W(V, B$–$V) = V - 3.06(B$–$V)$ and $W(V, B$–$I) = V - 1.34(B$–$I)$, where the coefficients were fixed according to the extinction law provided by Cardelli et al. (1989) calculated for the effective mean wavelengths of Landolt's (Landolt 1992) filter/photocathode combination for stars of spectral type A0III–F5III.

In their investigation Marconi et al. (2015) provided a detailed analysis of optical, optical-NIR and NIR period–Wesenheit–metallicity (PWZ) relations of the form $W(X, X$–$Y) = \alpha + \beta \cdot \log P + \gamma \cdot$ [Fe/H], where X and Y are magnitudes. They found that the coefficient of the metallicity term was smaller than $\sim$0.05 dex for the $W(V, B$–$V)$ and the $W(V, B$–$I)$ PWR (see their tables 7 and 8), indicating that the metallicity dependence of the V-band is counterbalanced by the convolution between the reddening vector and (B–V)–(B–I) colours.

The top-left panel of Fig. 3 shows the PWR(V, B–V) of the *clean* RRL sample. As expected *RRc* and *RRab* variables display
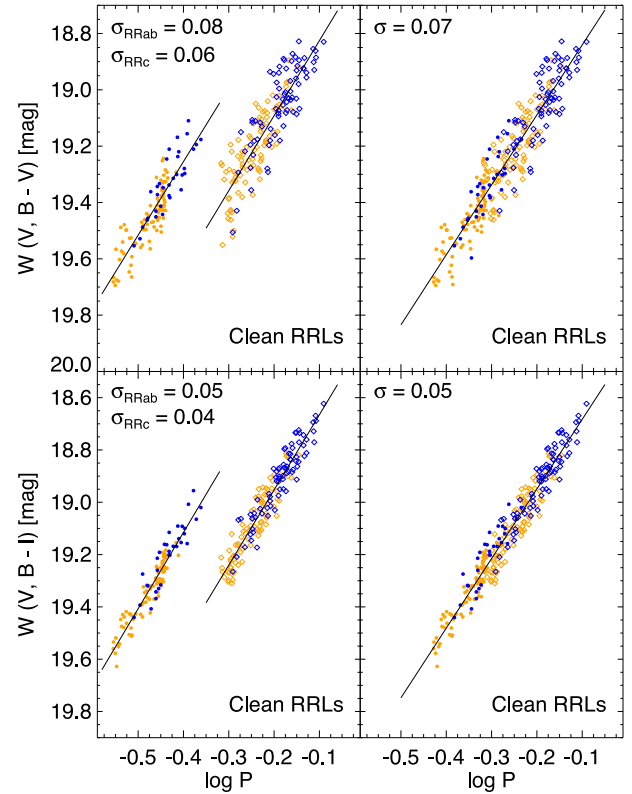

Figure 3. Top-left. Period–Wesenheit (V, B–V) relation for *RRab* and *RRc* RRLs of the *clean* sample. Symbols are the same as Fig. 1. Black lines display the least-squares fit of the two subsamples. The *sigma* of the fits are labelled. Top-right. Same as the left, but for the global (*RRab+RRc*) sample fundamentalized. Bottom-left. Same as the top-left, but for the PW (V, B–I) relation. Bottom-right. Same as the bottom left, but for the global RRL sample fundamentalized.

different PWRs. The vanishing dependence of the quoted PWRs on metallicity is further supported by the small dispersion in apparent Wesenheit magnitude of RRLs for each period. We performed a linear least squares fit to the three different subsamples and also applied a 3σ clip, and the final linear regressions are plotted as black lines in the top panels of Fig. 3. The coefficients of the empirical PWRs are listed in Table 1. To constrain the impact of using the *clean* sample on the empirical PWRs, the least-squares fit were also performed using the *full* RRL sample. Data listed in Table 1 clearly indicate that the coefficients of the PWRs attain similar values within the uncertainties.

We can see how the Bt-RRLs and Ft-RRLs follow the same relation. Moreover, Bt-RRLs seem to be the natural extension in the long-period regime of Ft-RRLs. The large sample of RRLs variables allows us to estimate the distance to Sculptor using three different PWRs for *RRc*, *RRab*, and the global sample (*RRc+RRab*, right-hand panel of Fig. 3). In deriving the distances of the global sample the periods of the RRc variables are fundamentalized, i.e. $\log P_{\mathrm{F}} = \log P_{FO} + 0.127$ (Bono et al. 2001; Marconi et al. 2015).

The bottom panels of Fig. 3 display the PWR for RRLs in Sculptor, but in the V, B–I bands (see Table 1). The standard deviations of the three different PWRs are slightly smaller than in V, B–V. The difference is mainly due to the fact that B–I is a better temperature indicator and the PWR closely mimics a period–luminosity–colour relation (Bono et al. in preparation).

Table 1. Parameters of the empirical fit, $W = \alpha + \beta \cdot \log P[\mathrm{mag}]$, performed on each group of RRL stars.

EM		CLEAN			FULL		
RRc	α	β	σ		α	β	σ
$W(V, B–V)$	18.21 ± 0.06	-2.61 ± 0.13	0.06		18.26 ± 0.05	-2.48 ± 0.10	0.06
$W(V, B–I)$	17.95 ± 0.05	-2.92 ± 0.10	0.04		18.05 ± 0.04	-2.65 ± 0.08	0.05
RRab	α	β	σ		α	β	σ
$W(V, B–V)$	18.56 ± 0.03	-2.66 ± 0.12	0.08		18.54 ± 0.02	-2.72 ± 0.10	0.09
$W(V, B–I)$	18.38 ± 0.02	-2.88 ± 0.07	0.05		18.38 ± 0.02	-2.83 ± 0.07	0.06
Global	α	β	σ		α	β	σ
$W(V, B–V)$	18.59 ± 0.02	-2.48 ± 0.05	0.07		18.58 ± 0.01	-2.50 ± 0.05	0.08
$W(V, B–I)$	17.42 ± 0.01	-2.66 ± 0.04	0.05		18.44 ± 0.01	-2.54 ± 0.03	0.06

Table 2. Parameters of the theoretical fit, $W(V, B–I) = \alpha + \beta \cdot \log P[\mathrm{mag}]$, performed following the procedure in Marconi et al. (2015) for metal-independent Wesenheit magnitudes.

TH $W(V, B–I)$	α	β	σ
RRc	-1.78 ± 0.06	-3.12 ± 0.13	0.06
RRab	-1.134 ± 0.008	-2.60 ± 0.04	0.07
Global	-1.134 ± 0.009	-2.48 ± 0.04	0.08

The distance estimates to Sculptor were derived using the three different subsamples (*RRab*, *RRc*, and global) and both the *clean, 290* and the *full, 471* RRL stars. In order to quantify the effect of both the zero-point (α) and the slope (β) of the relation on the distances, we adopted three different approaches: (i) theoretical – TH– in which we adopted predicted PWRs (see Marconi et al. 2015 and Table 2); (ii) semi-empirical – SE– in which we adopted the observed slopes listed in Table 1 and the theoretical zero-points; (iii) empirical – EM – in which we adopted the empirical slopes and where the zero-points are based on the field RRLs with HST trigonometric parallaxes (Benedict et al. 2011). In particular, we adopted RR Lyr itself to calibrate the *RRab* and the global sample, while the *RRc* were calibrated using RZ Cep. The mean B and V magnitudes provided by Coppola et al. (2015) and the individual distance moduli provided by Braga et al. (2015) and Neeley et al. (2015) have been used.

Using the empirical slopes and the above distances we estimated the zero-points for *RRab*, global and *RRc* PW relations (see Table 3). The former values for *RRab* and global relations agree quite well with predicted ones (-1.08 ± 0.01, -1.07 ± 0.01). However, in the case of the *RRc*, the new zero-points are ~30 per cent smaller than predicted (-1.56 ± 0.04).

Table 3 gives the distance moduli based on the *clean* and *full* RRL samples interpreted with the three different PWRs (*RRab*, *RRc*, global) and the three different calibrations (TH, SE, EM). The number of RRLs used to estimate the distance after the 3σ clipping is given in square brackets. Table 3 gives true distance moduli (mean values of μ ($V, B–V$) and μ ($V, B–I$) over the entire sample. For each fixed sample and approach, the estimated distance moduli agree with each other within 1σ and further support the evidence that the two *clean* and *full* samples give very similar distances. Since there is no reason a priori to prefer one of the five different estimates, for each sample we estimated the mean value — denoted by $<\mu>$ — that is given with the relative standard deviation (σ_μ). The distance determinations listed in Table 3 agree quite

well with similar distances available in the literature. In particular, they agree with the distance obtained by Pietrzynski et al. (2008) using RRLs [$19.67 \pm 0.02(0.12)$]. The difference is indeed smaller than 0.4σ. The true distance modulus to Sculptor was estimated as the mean among the mean distances of *RRc*, *RRab* and global sample. The mean distance based on the global sample is treated as an independent determination, because the *RRc*, once fundamentalized, become 'pseudo' fundamental pulsators (Braga et al. 2015). We found $<\mu>_{\mathrm{clean}} = 19.62$, $\sigma_\mu = 0.04$ and $<\mu>_{\mathrm{full}} = 19.63$, $\sigma_\mu = 0.06$ mag, respectively. We adopted the former one, for the reasons mentioned above.
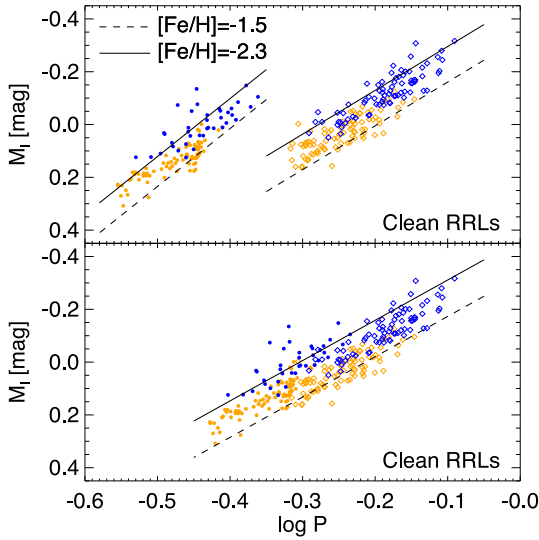
5 METALLICITY OF THE RRL STARS

5.1 Metallicity range

We will now take advantage of the new accurate distance determination to Sculptor [19.62, $\sigma_\mu = 0.04$] and the dependence of the *I*-band period–luminosity (PLI) relation on metallicity (Marconi et al. 2015) to constrain the metallicity distribution of the *clean* RRL sample. The top panel of Fig. 4 shows the comparison between RRLs and predicted PLI relations for two different metal abundances [Fe/H] $= -2.3$ (solid line) and [Fe/H] $= -1.5$ (dashed line). The majority of both *RRc* and *RRab* are bracketed by the quoted predictions. This evidence is further supported by the global sample (bottom panel). Moreover, the Bt-RRL and Ft-RRL subsample are located closer to the metal-poor and metal-rich relations, respectively. We performed the same test using the *full* sample and found that the metallicity ranges from ~ -2.4 to ~ -1.4 dex.

The spread in metallicity of the RRLs that we have measured using this method – 0.8 to 1.0 dex – is in excellent agreement with that obtained by Clementini et al. (2005) from spectroscopic measurements of RRL stars, but significantly smaller than the estimates based on spectroscopic metallicities of RGB stars. Measurements from LR spectra of 107 RRLs (ΔS parameter) indicate a mean Fe abundance of -1.83 ± 0.03 ($\sigma = 0.26$) with the metallicity ranging from ~ -2.40 to -0.85 dex (Clementini et al. 2005). However, they found only one metal-rich ([Fe/H] $= \sim -0.85$) RRL star while the bulk covers in a metallicity range from ~ -2.4 to -1.4 dex. Therefore, our estimates are in agreement with the bulk of the RRLs included in Clementini et al. (2005). More detailed spectroscopic measurements from medium resolution spectra for more than 300 RGBs revealed the occurrence of a metal-poor stellar component with Fe abundance ranging from -2.8 to -1.7 and of a metal-rich component with metallicity ranging from -1.7 to -0.9

Table 3. Distance moduli (in mag.) based on the current sample of RRL.

	CLEAN			FULL		
RRab	$\mu\,(V, B–V)$ [165]	$\mu\,(V, B–I)$ [164]	$\langle\mu\rangle$	$\mu\,(V, B–V)$ [261]	$\mu\,(V, B–I)$ [257]	$\langle\mu\rangle$
TH	$19.64 \pm 0.02(0.08)$	$19.57 \pm 0.01(0.05)$	–	$19.63 \pm 0.02(0.09)$	$19.57 \pm 0.01(0.06)$	–
SE	$19.64 \pm 0.02(0.08)$	$19.51 \pm 0.01(0.05)$	$19.59(0.05)$	$19.61 \pm 0.02(0.09)$	$19.52 \pm 0.01(0.06)$	$19.58(0.04)$
EM (α =[$-1.03 \pm 0.10; -1.04 \pm 0.10$])	$19.59 \pm 0.02(0.08)$	–	–	$19.58 \pm 0.02(0.09)$	–	–
RRc	$\mu\,(V, B–V)$ [116]	$\mu\,(V, B–I)$ [114]	$\langle\mu\rangle$	$\mu\,(V, B–V)$ [178]	$\mu\,(V, B–I)$ [177]	$\langle\mu\rangle$
TH	$19.70 \pm 0.02(0.06)$	$19.63 \pm 0.01(0.04)$	–	$19.69 \pm 0.02(0.06)$	$19.62 \pm 0.01(0.05)$	–
SE	$19.77 \pm 0.02(0.06)$	$19.73 \pm 0.01(0.04)$	$19.67(0.10)$	$19.82 \pm 0.02(0.08)$	$19.84 \pm 0.01(0.05)$	$19.70(0.14)$
EM (α =[$-1.31 \pm 0.17; -1.24 \pm 0.17$])	$19.52 \pm 0.02(0.06)$	–	–	$19.51 \pm 0.03(0.06)$	–	–
Global	$\mu\,(V, B–V)$ [279]	$\mu\,(V, B–I)$ [277]	$\langle\mu\rangle$	$\mu\,(V, B–V)$ [437]	$\mu\,(V, B–I)$ [429]	$\langle\mu\rangle$
TH	$19.66 \pm 0.02(0.07)$	$19.60 \pm 0.01(0.05)$	–	$19.65 \pm 0.02(0.08)$	$19.60 \pm 0.01(0.06)$	–
SE	$19.66 \pm 0.02(0.07)$	$19.55 \pm 0.01(0.05)$	$19.61(0.05)$	$19.65 \pm 0.02(0.08)$	$19.58 \pm 0.01(0.06)$	$19.61(0.04)$
EM (α =[$-0.98 \pm 0.09; -0.98 \pm 0.09$])	$19.57 \pm 0.02(0.07)$	–	–	$19.56 \pm 0.02(0.08)$	–	–
$<\mu>_{ADOPTED}$	–	–	$19.62(0.04)$	–	–	$19.63(0.06)$

Figure 4. Top. Absolute M_I period–luminosity relation for *RRab* and *RRc* variables of the clean sample. Symbols are the same as in Fig. 1. The dashed and solid black lines show predicted PLR for two different Fe abundances ([Fe/H]$= -1.5, -2.3$; (Marconi et al. 2015)). Bottom. Same as the top, but for the global sample.

(Tolstoy et al. 2004; Coleman, Da Costa & Bland-Hawthorn 2005). The empirical scenario was recently fortified by the extensive spectroscopic investigation based on medium resolution spectra of almost 400 RGBs by Kirby et al. (2009). They found a mean metallicity of -1.58 ($\sigma = 0.41$) with the Fe content ranging from ~ -3 to ~ -1 dex. Moreover, they also found evidence of a linear metallicity gradient.

However, we cannot exclude the possible occurrence of small samples of more metal-poor or metal-rich old stars, because these stellar components might produce HB stars either too hot or too cool to inhabit the RRL IS. This particularly means that RRLs are not sensitive to the possible occurrence of an extremely metal-poor component (Kirby et al. 2009; Starkenburg et al. 2013; Simon et al. 2015, see also Fig. 2). However, the lack of High Amplitude Short Period fundamental RRLs (HASP; log $P \leq -0.35$, $A_V \gtrsim 1$, Fiorentino et al. 2015) suggests that Sculptor does not host a significant metal-rich ([Fe/H] ≥ -1.3) old stellar population (Martínez-Vázquez et al. in preparation).

5.2 Radial properties

Tolstoy et al. (2004) found a radial gradient in the metallicity distribution of both RGB and HB stars, in the sense that the more metal-poor component is more spatially extended than the metal-rich one. Now, we will explore whether a radial gradient exists in the properties of the Sculptor RRL stars and whether it is associated with a metallicity gradient.

To avoid spurious fluctuations when moving from the innermost to the outermost regions we ranked the entire sample of RRL stars as a function of the radial distance. Then we calculated the running average by using a box starting with the first 200 more central objects in the list. We estimated the mean R_{HB},[2] radial distance and standard deviation in each successive sample of 200, removing five objects in the ranked list and adding five, until we reached the last 200 objects in the sample (651 RHBs, 536 RRLs, and 993 BHBs). We performed several tests changing both the number of objects included in the box and the step size and found that our conclusions are not affected. The data plotted in the top panel of Fig. 5 show that the value of R_{HB} parameter is steadily increasing over a substantial fraction of the body of the galaxy (r<25 arcmin), but flattens to RHB $\sim$0.55 in the outermost regions. The outermost regions display an almost constant HB morphology ($R_{HB}\sim$0.55). The steady increase in the R_{HB} suggests that we move from an HB mainly dominated by RRL and RHB stars ($R_{HB} \sim -0.1$) inside the core radius (r_c) to an HB mainly dominated by BHB stars and RRLs ($R_{HB} \sim 0.4$) beyond the half-light radius (r_h).

To further constrain the above intriguing evidence we also tested the radial trend of the ratio between Bt- and Ft-RRLs (*clean* sample), following the running average procedure with a sample size of 50, replacing five objects in the ranked list until we reached the last 50 objects in the sample of RRLs. The data plotted in the bottom panel show that the above ratio is quite constant ($N_{Bt}/N_{Ft} \sim 0.5$) inside the r_h, but it increases by a factor of 3 in the outermost regions ($r \sim 25$ arcmin). We cannot reach firm conclusions regarding a flattening in the outskirts of the galaxy ($r \sim 30$ arcmin) due to the limited sample of RRLs in these regions. The above findings therefore suggest that the metallicity gradient was already present >10 Gyr ago.

---

[2] We adopted the $R_{HB} = (B-R)/(B+V+R)$ parameter (Lee 1990), i.e. the ratio among stars that are located either inside (V = RRLs), or to the blue (B = BHBs), or to the red (R = RHBs) of the RRL IS.
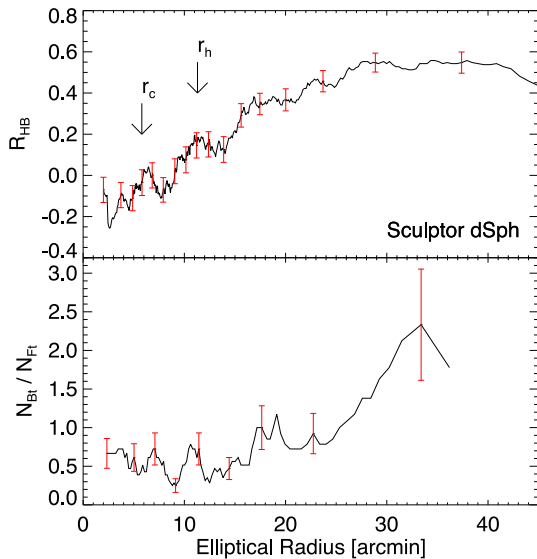
Figure 5. Top. The R_{HB} parameter as a function of the the elliptical radius. The vertical arrows mark the core ($r_c = 5.8$ arcmin, Mateo 1998) and half-light radius ($r_h = 11.3$ arcmin, Irwin & Hatzidimitriou 1995). The vertical red lines display the errors on R_{HB} based on Monte Carlo simulations. The Bottom. Same as the top, but for the ratio between bright and faint RRLs in the *full* sample.

6 CONCLUSIONS

We have performed detailed multiband homogeneous optical photometry of the Sculptor dSph. We accumulated more than 4400 images (proprietary plus archive images) covering a time interval of ∼24 years. The precision of the photometry and the accuracy of both the absolute and relative zero-points allowed us to provide new mean magnitudes for 574 variable stars. Among them 536 have been identified as Sculptor RRLs: 82 are new identification while for 219 candidates we provide for the first time the pulsation parameters. The new RRL data set allowed us to investigate several interesting open problems.

(i) *True distance modulus*. The use of three photometric bands and of two diagnostics, the PWRs in *V*, *B–V*, and in *V*, *B–I*, that are reddening free and only minimally affected by metal content, allowed us to provide very accurate distances. The errors on individual distance modulus are never larger than 0.02_{sys} and 0.09_{ran}. To investigate possible systematics affecting the quoted diagnostics, we have adopted three independent calibrations, named empirical, semi-empirical, and theoretical. We ended up with a mean distance moduli of 19.62 with $\sigma_\mu = 0.04$ using the *clean* (290) sample. All the estimates presented in this paper agree quite well with similar evaluations based on reliable distance indicators (Pietrzynski et al. 2008).

(ii) *Metallicity range*. We used the *I*-band PLR of RRL to constrain the metallicity range covered by Sculptor RRLs. The *clean* RRL subsample suggests that the Fe content of the old (t>10Gyr) stellar population ranges from −2.3 to −1.5 dex. This range is in excellent agreement with spectroscopic measurements of RRLs, but significantly narrower than the distribution of RGB metallicities ($-3.0 \lesssim$ [Fe/H] $\lesssim -0.8$ dex; Kirby et al. 2009).

(iii) *HB morphology*. The use of homogeneous and accurate photometry covering a significant fraction of the body of the galaxy allowed us to constrain the HB parameter as a function of radius. We found that the HB morphology changes from −0.1 (dominated

by BHB stars and RRL) to +0.55 (dominated by RHB stars and RRL) when moving from the innermost to the outermost galactic regions, as expected from the presence of a younger and/or more metal-rich stellar population in the centre of the galaxy (e.g. de Boer et al. 2012).

(iv) *RRL luminosity distribution*. We split the RRL sample into Bt-RRL ($V \leq 20.13$ mag) and Ft-RRL ($V > 20.13$ mag) sub-samples. The large sample of RRLs allowed us to constrain the radial gradient of the Bt/Ft RRL ratio. We found that this ratio is almost constant in the innermost regions while it shows a steady increase for radial distance ranging from r_h to 25 arcmin. In passing we note that this is, to our knowledge, the first clear evidence in which HB stars and RRLs display similar radial trends. Analogous empirical evidence was found in the Tucana dSph (Bernard et al. 2008). However, a dichotomous population of RRLs was clearly identified there.

This work shows that RRLs provide significant constraints on the chemical enrichment history of its host galaxy. In particular, the combination of a large sample – one of the largest RRL samples in a dSph galaxy to date (Bersier & Wood 2002; Monelli et al. 2012) – with high quality, multiband photometry allowed us to determine the metallicity distribution of the old stellar component, and revealed the presence of a significant metallicity gradient among the oldest stars (>10 Gyr). Our results are in agreement with the star formation history of Sculptor recently obtained by de Boer et al. (2012), the synthetic HB modelling of Salaris et al. (2013), as well as the various works based on spectroscopic data (see e.g. Tolstoy et al. 2004; Battaglia et al. 2008; Kirby et al. 2009). In particular, we find that Sculptor underwent a very efficient chemical enrichment: the metallicity range of RRLs shows an increase in the Fe content by almost one dex in less than 2–3 Gyr. The metallicity gradient suggests that star formation lasted until more recently in the inner regions, therefore further enriching the interstellar medium. However, we cannot exclude the possibility of a merger at an early epoch, or tidally-induced heating of an initially disc-like structure into an spheroid (Mayer et al. 2001, 2006) as the origin of the gradient.

REFERENCES

Baade W., Hubble E., 1939, PASP, 51, 40
Battaglia G., Irwin M., Tolstoy E., Hill V., Helmi A., Letarte B., Jablonka P., 2008, MNRAS, 383, 183
Benedict G. F. et al., 2011, AJ, 142, 187
Bernard E. J. et al., 2008, ApJ, 678, L21
Bernard E. J. et al., 2009, ApJ, 699, 1742
Bersier D., Wood P. R., 2002, AJ, 123, 840

Blazhko S., 1907, Astron. Nachr., 175, 327

Bono G., Caputo F., Castellani V., Marconi M., Storm J., 2001, MNRAS, 326, 1183

Bono G., Caputo F., Castellani V., Marconi M., Storm J., Degl'Innocenti S., 2003, MNRAS, 344, 1097

Braga V. F. et al., 2015, ApJ, 799, 165

Cacciari C., Clementini G., 2003, in Alloin D., Gieren W., eds, Lecture Notes in Physics, Vol. 635, Stellar Candles for the Extragalactic Distance Scale. Springer-Verlag, Berlin, p. 105

Cardelli J. A., Clayton G. C., Mathis J. S., 1989, ApJ, 345, 245

Catelan M., Pritzl B. J., Smith H. A., 2004, ApJS, 154, 633

Clementini G., Gratton R., Bragaglia A., Carretta E., Di Fabrizio L., Maio M., 2003, AJ, 125, 1309

Clementini G., Ripepi V., Bragaglia A., Martinez Fiorenzano A. F., Held E. V., Gratton R. G., 2005, MNRAS, 363, 734

Coleman M. G., Da Costa G. S., Bland-Hawthorn J., 2005, AJ, 130, 1065

Coppola G. et al., 2015, preprint (arXiv:1509.02687)

Da Costa G. S., 1984, ApJ, 285, 483

Dambis A. K., Rastorguev A. S., Zabolotskikh M. V., 2014, MNRAS, 439, 3765

de Boer T. J. L. et al., 2012, A&A, 539, A103

Fiorentino G. et al., 2015, ApJ, 798, L12

Gallart C., Zoccali M., Aparicio A., 2005, ARA&A, 43, 387

Hodge P. W., 1965, ApJ, 142, 1390

Hurley-Keller D., Mateo M., Grebel E. K., 1999, ApJ, 523, L25

Irwin M., Hatzidimitriou D., 1995, MNRAS, 277, 1354

Kaluzny J., Kubiak M., Szymanski M., Udalski A., Krzeminski W., Mateo M., 1995, A&AS, 112, 407

Kirby E. N., Guhathakurta P., Bolte M., Sneden C., Geha M. C., 2009, ApJ, 705, 328

Klein C. R., Richards J. W., Butler N. R., Bloom J. S., 2014, MNRAS, 440, L96

Kunkel W. E., Demers S., 1977, ApJ, 214, 21

Landolt A. U., 1992, AJ, 104, 340

Layden A. C., Ritter L. A., Welch D. L., Webb T. M. A., 1999, AJ, 117, 1313

Lee Y.-W., 1990, ApJ, 363, 159

Madau P., Dickinson M., 2014, ARA&A, 52, 415

Madore B. F. et al., 2013, ApJ, 776, 135

Majewski S. R., Siegel M. H., Patterson R. J., Rood R. T., 1999, ApJ, 520, L33

Marconi M. et al., 2015, ApJ, 808, 50

Mateo M. L., 1998, ARA&A, 36, 435

Mayer L., 2010, Adv. Astron 2010, 25

Mayer L., Governato F., Colpi M., Moore B., Quinn T., Wadsley J., Stadel J., Lake G., 2001, ApJ, 547, L123

Mayer L., Mastropietro C., Wadsley J., Stadel J., Moore B., 2006, MNRAS, 369, 1021

Monelli M. et al., 2012, MNRAS, 422, 89

Neeley J. R. et al., 2015, ApJ, 808, 11

Pietrinferni A., Cassisi S., Salaris M., Castelli F., 2004, ApJ, 612, 168

Pietrzynski G. et al., 2008, AJ, 135, 1993

Rizzi L., 2002, PhD thesis, Univ. Padova, Italy

Salaris M., de Boer T., Tolstoy E., Fiorentino G., Cassisi S., 2013, A&A, 559, A57

Shapley H., 1938, Harv. Coll. Obs. Bull., 908, 1

Simon J. D., Jacobson H. R., Frebel A., Thompson I. B., Adams J. J., Shectman S. A., 2015, ApJ, 802, 93

Smith G. H., Dopita M. A., 1983, ApJ, 271, 113

Starkenburg E. et al., 2013, A&A, 549, A88

Stetson P. B., 1987, PASP, 99, 191

Stetson P. B., 1994, PASP, 106, 250

Stetson P. B. et al., 1998, ApJ, 508, 491

Storm J., Carney B. W., Gieren W. P., Fouqué P., Latham D. W., Fry A. M., 2004, A&A, 415, 531

Thackeray A. D., 1950, The Observatory, 70, 144

Tolstoy E. et al., 2004, ApJ, 617, L119

Tolstoy E., Hill V., Tosi M., 2009, ARA&A, 47, 371

Udalski A., Szymanski M., Kaluzny J., Kubiak M., Mateo M., 1992, Acta Astron., 42, 253

van Agt S. L. T. J., 1978, Publ. David Dunlap Obs., 3, 205

Walker M. G., Mateo M., Olszewski E. W., Gnedin O. Y., Wang X., Sen B., Woodroofe M., 2007, ApJ, 667, L53

Walker M. G., Mateo M., Olszewski E. W., Sen B., Woodroofe M., 2009, AJ, 137, 3109

Welch D. L., Stetson P. B., 1993, AJ, 105, 1813

This paper has been typeset from a TeX/LaTeX file prepared by the author.